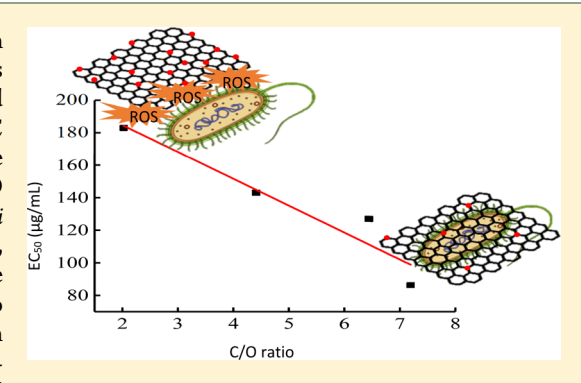


Structure—Property—Toxicity Relationships of Graphene Oxide: Role of Surface Chemistry on the Mechanisms of Interaction with **Bacteria**

Ana C. Barrios, †,‡ Yan Wang, Leanne M. Gilbertson, and François Perreault*,†,‡®

Supporting Information

ABSTRACT: Graphene oxide (GO) is an antimicrobial agent with tunable surface chemistry. To identify the physicochemical determinants of GO's antimicrobial activity, we generated different modified Hummer's GO materials thermally annealed at 200, 500, or 800 °C (TGO200, TGO500, and TGO800, respectively) to modify the surface oxygen groups on the material. Plating assays show that as-received GO (ARGO) and TGO200, TGO500, and TGO800 reduce Escherichia coli viability by 50% (EC₅₀) at 183, 143, 127, and 86 μ g/mL, respectively, indicating higher bacterial toxicity as ARGO is reduced. To uncover the toxicity mechanism of GO, fluorescent dye-based assays were used to measure oxidative stress at the EC50. ARGO showed an increase in intracellular reactive oxygen species, measured as an increase in 2',7'dichlorodihydrofluorescein diacetate fluorescence, whereas TGO500 and



TGO800 induced an increase in the fluorescence of fluorescein diacetate (FDA) by 30 and 42%, suggesting a decrease in cell permeability. Because of a possible wrapping mechanism, plating assays after post-exposure sonication were performed to explain TGO's low oxidative response and high FDA levels. Results show no difference in colony-forming units, indicating that inhibition of cell growth is a result of the adsorption of bacterial cells on the GO material. By comparing different GO samples at their EC₅₀, this study reveals that reduction of GO alters both the mechanisms of cellular interaction and the degree of toxicity to bacteria.

1. INTRODUCTION

Carbon can take multiple allotrope forms, ranging from the three-dimensional diamond to the zero-dimensional fullerene, each with unique physicochemical properties. Since the first isolation of graphene in 2004,² a two-dimensional (2-D) allotrope of carbon, graphene, has gained popularity because of its high electron mobility, thermal conductivity, mechanical strength, and surface area.^{3,4} Graphene oxide (GO), the oxidized form of graphene, is a carbon nanomaterial (CNM) that consists of a single layer of carbon atoms arranged in a hexagonal network where most of the carbon atoms preserve sp² hybridization. It is decorated with a high density of oxygen functional groups including epoxide and hydroxyl moieties on the basal planes and carboxylic and carbonyl groups at the edges. The presence of oxygen in the carbon structure greatly reduces the conductivity and mechanical properties of GO compared to that of graphene. However, because of its simple synthesis and flexible chemistry, GO has been a popular building block of many composite CNMs.4

In the last decade, several studies have shown the antimicrobial properties of GO when exposed to a wide array of microorganisms, including Gram-positive and -negative bacteria. 6-9 Multiple mechanisms are involved when bacterial cells come in contact with graphene-based materials, that is, membrane stress, oxidative stress, and/or wrapping isolation. 10-12 Each of these mechanisms can act independent of each other or together to inhibit bacterial growth through chemical or physical interactions. 10,11,13-15 Cellular injury might occur from the impact of physical membrane disruption, creating an irreversible destruction of the cells after exposure to CNMs.¹⁴ The action of oxidative stress on bacteria results in the oxidation of lipids, nucleic acids, and proteins, which can eventually lead to cell membrane destruction and cellular growth inhibition through the generation of reactive oxygen species (ROS).¹¹ Lastly, bacterial cells can be biologically isolated from their growth medium when graphene sheets enclose them, thus preventing

Received: August 22, 2019 Revised: October 30, 2019 Accepted: November 7, 2019 Published: November 7, 2019



 $^{^\}dagger$ School of Sustainable Engineering and the Built Environment and ‡ Nanosystems Engineering Research Center for Nanotechnology-Enabled Water Treatment, Arizona State University, Tempe 85287-3005, Arizona, United States

 $^{^{\}S}$ Department of Civil and Environmental Engineering and $^{\parallel}$ Department of Chemical and Petroleum Engineering, University of Pittsburgh, Pittsburgh 15260, Pennsylvania, United States

nutrient consumption and growth, leading to cell death. 16,17 However, cell inhibition by GO wrapping seems reversible, and the viable cells may be recovered when separated from GO via sonication. 11,17

The structure and surface chemistry of CNMs play an important role when determining their antimicrobial mechanism. Previous research on carbon nanotubes (CNTs) and fullerenes demonstrated that their toxicity is linked to their physicochemical properties and that changes in size, functionalization, and oxidation levels alter their toxicity potential. 18-22 Arias and Yang found that single-walled CNTs (SWCNTs) with hydroxyl and carboxylic surface groups exhibited stronger antimicrobial activities toward Salmonella typhimurium, Bacillus subtilis, and Staphylococcus aureus when compared to SWCNTs functionalized with amines.²³ Gilbertson et al. demonstrated that by manipulating the surface chemistry of multi-walled CNTs, one can control the electrochemical and biological activities of the material. 18,22 Recently, multiple studies have focused on developing a framework that serves as a guideline for the sustainable selection and design of nanomaterials, including CNTs.²⁴⁻

Based on the synthesis method used, GO materials can have large differences in oxygen content, sheet size, morphology, hydrophilicity, and dispersibility that may impact GObacteria interactions and consequently GO's toxicity toward microorganisms. When the effect of GO and reduced GO (rGO) $(0-200 \mu g/mL)$ was compared using Pseudomonas aeruginosa as a model organism, Gurunathan et al. observed a loss in cell viability in a dose- and time-dependent manner through the generation of ROS and a significant production of superoxide radical anion (O^{2-}) . A study by Liu et al. showed that a GO dispersion had the highest antibacterial activity toward Escherichia coli (E. coli) with 89.7% loss of viability at 40 μ g/mL, followed by rGO, graphite, and graphite oxide. The toxicity was attributed to the smaller size of GO sheets compared to that of the other materials, as well as membrane and oxidative stress.²⁸ Similarly, Perreault et al. observed a 4fold increase in the antimicrobial effect of a GO-coated surface when the sheet area decreased from 0.65 to 0.01 μ m². Additionally, Akhavan and Ghaderi showed that rGO nanowalls were more toxic toward both E. coli and S. aureus than the unreduced GO nanowalls, where only 41 and 16% of the bacteria survived after 1 h contact with GO and rGO nanowalls, respectively.²⁹ This effect was attributed to the better charge transfer between the bacteria and the sharper edges of the reduced nanowalls. 29 However, using lipid bilayers to study the interaction of 2-D nanomaterials with membranes, Zucker et al. showed that physical interactions leading to lipid extraction were more important than chemical mechanisms for membrane disruption.³⁰ Therefore, multiple studies related the material's structure to its antimicrobial potency, often with contradictory findings. A direct comparison between oxidized and reduced form of GO can be challenging because of the effect of GO's surface chemistry on aqueous stability, electron conductivity, and mechanical properties, all of which influence cellular interactions. As a result, how the properties of GO change the way this material interact with cells remains unresolved.

In this study, we investigate how changes in the surface chemistry between a modified Hummer's GO (ARGO) and thermally annealed GO (TGO200, 500, and 800) alter the mechanisms of antimicrobial activity toward E. coli. The dependency between the oxygen content and antimicrobial

activity is demonstrated by calculation of the effective concentration (EC₅₀). Then, by comparing materials on the same biological endpoint (i.e., EC₅₀ concentration), the mechanisms involved in GO-bacteria interaction could be examined and explained using fluorescent dye assays indicative of oxidative stress and membrane permeability. The findings in this study aim to highlight the antimicrobial properties and mechanisms of graphene-based materials, which can then provide insights into the safe design of CNMs through the establishment of relationships that relate the materials' chemical structure and properties to their function and inherent hazard.

2. MATERIALS AND METHODS

2.1. Materials and Chemicals. 2.1.1. Chemicals. The fluorescent dyes: propidium iodide (PI) and SYTO 9 (from the LIVE/DEAD BacLight bacterial viability kit), BODIPY 493/503 (4,4-difluoro-1,3,5,7,8-pentamethyl-4-bora-3a,4adiaza-s-indacene), 2',7'-dichlorodihydrofluorescein diacetate (H₂DCFDA), and fluorescein diacetate (FDA) were obtained from Thermo Fisher Scientific (Molecular Probes, Eugene, OR). Unless specified, all chemicals were dissolved in deionized (DI) water obtained from a GenPure UV xCAD plus ultrapure water purification system (Thermo Scientific, Waltham, MA).

2.1.2. Graphene Oxide. A modified Hummer's powdered single layer GO (~99% pure) was purchased from ACS Materials LLC (Medford, MA, USA, product no. GNOP10A5) and used as received (ARGO).

2.1.3. Thermally Annealed rGO. Surface modification on GO was prepared by thermally treating ARGO under helium (He) gas flow in a tube furnace (Thermo Scientific Lindberg/ Blue M TF55035A-1) with a custom-built quartz tube at increasing temperatures 200, 500, and 800 °C. 27 ARGO was added to the quartz tube and heated at a rate of 5 °C min⁻¹ to the maximum temperature, held for 30 min, and left to cool at room temperature under He flow. These thermally annealed rGO samples are referred to as TGO200, TGO500, and TG800, respectively.

2.2. Material Characterization. ARGO and TGOs were characterized using X-ray photoelectron spectroscopy (XPS), to quantify the surface chemistry and distribution of functional groups, and scanning electron microscopy (SEM), to determine the GO size flake. For XPS analysis, the sample holder was covered with a double-sided copper tape and dusted with enough GO powdered material. The sample was then loaded into a Thermo Scientific ESCALAB 250Xi that uses a monochromatic Al K α X-ray source with the following parameters: 1486.7 eV and a spot size of 650 μ m. Survey spectra were collected using a 150 eV pass energy and a 1.0 eV step size. The high-resolution C 1s spectra were collected using a 50 eV pass energy and a 0.1 eV step size. Three measurements in different locations of each sample were collected. The Thermo Scientific Avantage software was used for peak fitting and to calculate the atomic percentage.²⁷ SEM images were taken with an Amray 1910 field emission scanning electron microscope using 10 eV. For sample preparation, 3 μ L of a diluted 50 μ g/mL GO stock solution was drop-cast on a 1 cm × 1 cm silicon wafer previously cleaned via UV-ozone treatment for 20 min (UV/Ozone ProCleaner, BioForce Nanosciences, Ames, IA). 11 The software ImageJ was used to process the SEM images and measure GO dimensions.

2.3. Antimicrobial Activity of GO in Suspension. Before the microbiological tests, all glassware and media were sterilized by autoclaving at 121 °C for 2 h. E. coli W3110 (American Type Culture Collection ATCC 11303) was grown overnight in Lysogeny Broth (LB) at 37 °C on a shaker plate at 140 rpm in an Isotemp incubator (Fisher Scientific). This bacterium was selected for its wide applications in environmental engineering as a model indicator³¹ and its welldocumented interactions with CNMs, simplifying the comparison between previously published research and this study. The culture was then diluted in fresh LB (1:25) and grown under the same conditions until the optical density reached 1. indicating log phase (\sim 2 h). Bacterial cells were washed by centrifugation three times with sterile 0.9% NaCl solution before being diluted to 10⁷ colony-forming units (CFUs)/mL in sterile saline solution.

For GO exposure to the bacteria, stock suspensions of ARGO and each TGO material were made in nanopure water (5000 µg/mL) and bath-sonicated for 1 h (M3800 Branson Ultrasonic Corporation, Danbury, CT). In 7 mL scintillation vials, 3.5 mL of sterile 0.9% NaCl, 0.5 mL of clean bacteria solution, and the required volume of each GO suspension were added to reach concentrations from 1, 10, 50, 150, 250, and 500 μ g/mL in a total volume of 5 mL. For all experiments, a negative control (no GO added) treatment was created by adding 1 mL of sterile DI water. The positive control was prepared by adding 500 μ L of 50 mM CuCl₂ and 500 μ L of sterile DI water for a total concentration of 5 mM CuCl₂ in a volume of 5 mL. CuCl₂ was used as a positive control because it is known to be an antimicrobial agent. 32 Vials were placed on a horizontal shaker (Branstead Lab-Line) at 80 rpm for 3 h and kept at room temperature. After the 3 h contact time, the bacteria-GO suspensions were diluted (1:10) in Eppendorf tubes and vortexed, and 50 μ L of each suspension was spread on a LB agar plate and incubated overnight at 37 °C for CFU enumeration. To assess GO entrapment around bacteria cells, a postsonication experiment was done. After the 3 h contact time and plating, each Eppendorf tube containing the diluted bacteria-GO suspension was bath-sonicated for 10 min as previously described, 17 and 50 μ L of the suspension was immediately plated and incubated in the same conditions.

2.4. Effective Concentration Calculation. The halfmaximum effective concentration (EC50) was determined in OriginPro 8.5.1 software using a sigmoidal fit of the doseresponse function with the equation

$$y = A1 + \frac{A2 - A1}{1 + 10^{(\log_x 0 - x)p}}$$
 (1)

where A1 = bottom asymptote, A2 = top asymptote, $log_x 0 =$ center, and p = hill slope, and EC₅₀ is given by

$$EC_{50} = 10^{\log_x 0} \tag{2}$$

2.5. Determination of Viable Cells after GO Exposure. Cell viability in GO-bacteria suspensions was determined by LIVE/DEAD fluorescent staining. After the 3 h exposure time, cells were stained by adding 1 μ L of 3.34 mM SYTO 9 and 1 μ L of 20 μ M PI to 1 mL of suspension. The samples were incubated for 30 min in the dark before pipetting 5 μ L of each sample in a microscope slide for epifluorescence microscopy. Ten pictures per replicate were taken with a Leica DM6 epifluorescence microscope (Leica Microsystems Inc. Buffalo Grove, IL). A visual confirmation of the association of E. coli

with GO was obtained using SEM with a JSM 6300 scanning electron microscope (JEOL USA, Peabody, MA) operated at 15 kV, and images were captured with an IXRF Systems model 500 digital processer (IXRF System Inc., Austin, TX). Briefly, for sample preparation, samples were suspended in 2% glutaraldehyde buffered with 0.1 M sodium phosphate, pH 7.2 overnight at 4 °C and then washed 3× in the same buffer. Secondary fixation was done with 1% osmium tetroxide in buffer for 1 h at room temperature. The samples were washed 3× with DI water and adhered to poly-L-lysine-coated coverslips, washed, and then treated with an ascending series of acetone solutions, leading to complete dehydration. Criticalpoint drying was done with a CPD-020 unit (Balzers-Union, Principality of Liechtenstein) using liquid carbon dioxide. The dried samples on coverslips were mounted on aluminum stubs and coated with approx. 10-12 nm of gold-palladium using a Hummer II sputter coater (Technics, San Jose, CA).

2.6. Esterase Activity after GO Exposure. Changes in esterase activity or membrane damage in GO-bacteria suspensions were estimated using the FDA fluorescent dye.³⁴ FDA is a nonpolar ester that passes through cell membranes. Once inside the cell, FDA is hydrolyzed by esterase, an enzyme present in viable cells, to produce fluorescein, which accumulates inside the cell and fluoresces under UV light.³⁵ After the 3 h exposure time, cells were stained with 5 mM FDA in 1 mL of GO-bacteria suspension. The samples were incubated for 30 min in the dark before pipetting 200 µL of each sample in a 96-well plate. The fluorescence was measured using an excitation wavelength of 490 nm and an emission wavelength of 526 nm. All the fluorescence data were collected using a fluorescence plate reader (Synergy H1, BioTek). Data were expressed as the mean fluorescence intensity and the results as a percentage with respect to the control.

2.7. ROS Generation after GO Exposure. ROS formation was measured using the cell permeable indicator H₂DCFDA.³⁶ Cellular esterases hydrolyze the probe to the nonfluorescent 2',7'-dichlorodihydrofluorescein (H₂DCF), which is better retained in the cells. In the presence of ROS and cellular peroxidases, H2DCF is transformed to the highly fluorescent 2',7'-dichlorofluorescein (DCF). An H₂DCFDA stock solution (10 mM) was prepared in ethanol in the dark. After the 3 h exposure time, 1 mL of bacterial samples was exposed to 0.2 mM H₂DCFDA and incubated for 15 min in the dark before pipetting 200 μ L of each sample in a 96-well plate. The DCF fluorescence was measured using an excitation wavelength of 495 nm and an emission wavelength of 527 nm.

2.8. Determination of Lipid Peroxidation after GO **Exposure.** Lipid peroxidation was measured using the cell permeable indicator BODIPY 493/503. After the 3 h exposure time, 1 mL of bacterial samples was exposed to 10 μ L of a 2 mM BODIPY solution.³⁴ The samples were incubated for 30 min in the dark before pipetting 200 μ L of each sample in a 96well plate. The fluorescence was measured using an excitation wavelength of 488 nm and an emission wavelength of 510 nm.

2.9. Glutathione (GSH) Oxidation after GO Exposure. Thiol concentration was quantified following Ellman's assay³⁷ as per previous studies. ^{11,18,19,27} GO dispersions of 50 μ g/mL were prepared by bath sonication (VWR Aquasonic 150T) for 30 min in a 33 mM bicarbonate buffer with a pH of 8.6. A stock GSH solution was added to the triplicate samples to reach a final concentration of 0.4 mM. The samples were covered with aluminum foil to avoid oxidation induced by the light and placed on a rotator at room temperature until the

Table 1. Compiled XPS Data Representing the Atomic Percent of the Carbon and Oxygen Content and the C/O Atomic Ratio, Determined from the Component Fitting of the C 1s Envelope for ARGO and TGO Samples^a

samples	C %	O %	C/O	% sp ² C	% C-O	% C=O	% СООН
ARGO	$65.85 \pm 0.80^{\circ}$	32.53 ± 0.54^{a}	$2.02 \pm 0.06^{\circ}$	37.23 ± 1.14	41.89 ± 0.66	15.66 ± 2.09	5.24 ± 0.29
TGO200	80.36 ± 0.21^{b}	18.23 ± 0.10^{b}	4.41 ± 0.03^{b}	70.76 ± 0.01	18.35 ± 0.30	5.22 ± 0.08	5.68 ± 0.23
TGO500	84.76 ± 1.39^{a}	13.16 ± 1.09^{c}	6.48 ± 0.62^{a}	75.75 ± 1.43	16.67 ± 1.62	5.06 ± 0.18	2.53 ± 0.01
TGO800	83.30 ± 0.44^{a}	11.59 ± 0.18^{c}	7.19 ± 0.11^{a}	84.71 ± 0.22	9.09 ± 0.36	4.58 ± 0.37	1.62 ± 0.24

[&]quot;Different letters represent statistical significance between materials at $p \le 0.05$ (n = 3). Trace amounts of impurities were also found and compiled in Table S1

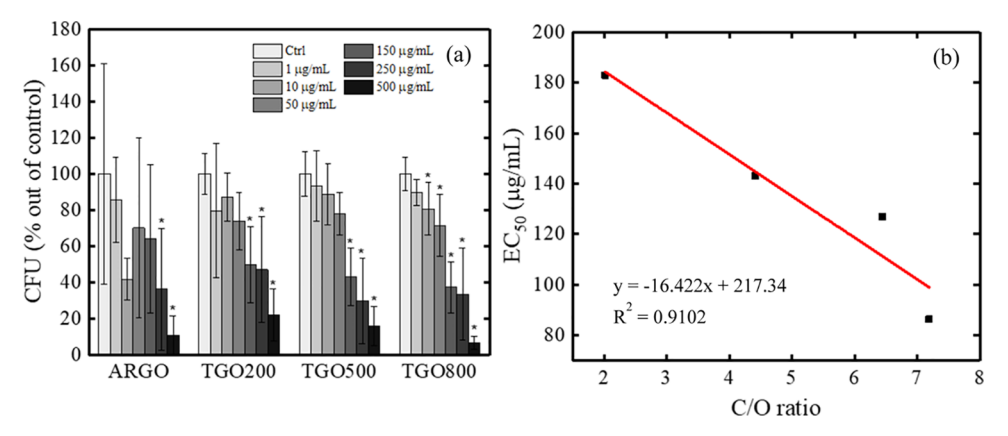


Figure 1. Antimicrobial activity of GO to *E. coli*. (A) Plating assay results after 3 h of contact time between GO and *E. coli* using $0-500 \mu g/mL$ of the material. (B) Linear fit of EC_{50} values of ARGO and annealed GO and C/O ratios. Stars (*) represent statistical difference with respect to control. All experiments are compared to the negative control (no GO), whereas the positive control (CuCl₂) is not shown because there was no bacteria growth (n = 9).

experiment was done (6 h). An aliquot was removed at 0, 1, 2.5, 4, and 6 h and filtered using a 0.22 μ m syringe filter. Ellman's reagent, 5,5'-dithiobis(2-nitrobenzoic acid), which reacts with thiol groups of GSH to produce 3-thio-6-nitrobenzoate (TNB), was added. The absorbance was measured at 412 nm using an extinction coefficient of 14 150 $\rm M^{-1}~cm^{-1}$ and then used to calculate the concentration of GSH remaining in solution. The percent loss of GSH was calculated by comparing the results with the negative control (no GO).

2.10. Data Analysis and Statistics. All treatments were prepared in triplicate and repeated at least in three independent experiments. Means and standard deviations were calculated for each treatment. Significant differences between control samples (no GO) and GO-exposed bacterial samples were determined via a one-way analysis of variance (ANOVA), followed by a Tukey post-hoc test where a *p* value less than 0.05 was considered to be significant. Statistical analysis was done using the Statistical Package for Social Sciences software version 25.

3. RESULTS AND DISCUSSION

3.1. Surface Chemistry Characterization of ARGO and TGOs. The different GO materials were characterized by XPS to identify how the surface chemistry of GO influences the interactions of GO with bacteria. XPS offers a quantitative approach to evaluate the reduction degree of GO and the changes in types of oxygen functionalities as a function of thermal reduction. Table 1 shows the relative percentage of carbon, oxygen, and their different bonds for all samples. The relative percentage of carbon (C %) in all annealed materials increases significantly with the increasing annealing temperatures and ranges from 66 to 83% from ARGO to TGO800,

accompanied with a decrease of percent oxygen (O %) from 33 to 12%. The observed increase in C/O ratio confirms successful deoxygenation of the GO surface and indicates restoration of the conjugated carbon structure. 38

Moreover, peak deconvolution of the C 1s spectra can determine the relative presence of different carbon-oxygen bonds in GO. The deconvolution of C 1s results in four peaks approximately located at binding energies of 284.8, 286.3, 287.5, and 288.8 eV, which are assigned to single and double carbon bonds (sp² C), epoxide and hydroxyl (C-O), carbonyl (C=O), and carboxylate (COOH) functional groups, respectively (Figure S1). The assignments and binding energies are in agreement with previous studies. 5,27,39-42 The content of C-O groups, including epoxide and hydroxyl groups on the GO basal plane, decreases from 41.89% for ARGO to 9.09% for TGO800 upon thermal annealing. This decrease can be attributed to the reduction of epoxide groups, which are the most abundant on GO surfaces^{27,38} and lack chemical and thermal stability.²⁷ At higher temperatures (800 °C), C-O bonding contributes the highest fraction (9.09%) compared to C=O and COOH (4.58 and 1.62%, respectively). This has been observed in previous studies and is attributed to the higher thermal stability of C-OH groups intercalated into graphene interlayers. 27,38 The C=O and COOH groups, which are mostly found in the edges of the GO structure, exhibit a steady decrease upon thermal reduction.

In addition to surface chemistry analyses, potential changes in the GO sheet size were evaluated because of its role in the antimicrobial activity of GO. 11,14,16,28 SEM imaging showed that thermal annealing of GO had no significant effect on the sheet size. The average lateral sizes of ARGO and TGO800 were 1.19 \pm 0.71 and 1.11 \pm 0.74 $\mu \rm m$, respectively. The size and image processing was done using ImageJ and is based on

Environmental Science & Technology

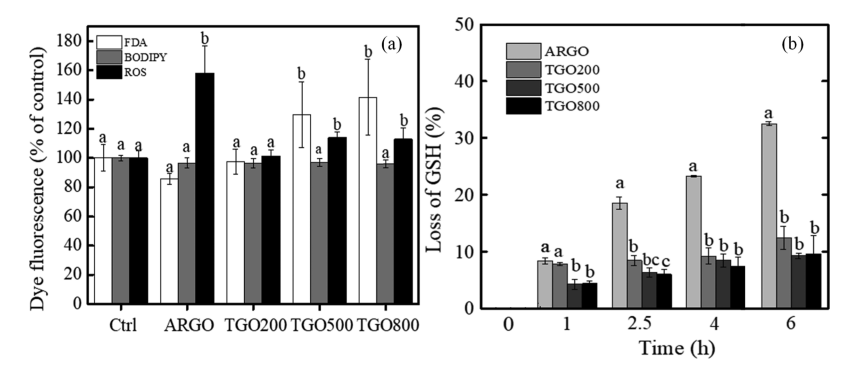


Figure 2. Biochemical response of ARGO and annealed GO in *E. coli* after 3 h of exposure at the EC₅₀ concentration. (A) Fluorescent dye assays showing esterase activity, lipid peroxidation, and ROS generation. A 5 mM CuCl₂ was used as a positive control depicted as (+), whereas the negative control (Ctrl) had no GO. (B) Time-dependent GSH oxidation mediated by GO materials. The mass loading of the materials is 50 μ g/mL. Different letters represent statistical difference at $p \le 0.05$ when compared to the control (n = 9). All experiments are compared to the negative control (no GO).

the analysis of approximately 100 sheets captured from multiple images (Figure S2).

3.2. Antimicrobial Activity of ARGO and TGOs Related to Their Surface Chemistry. The antimicrobial properties of ARGO and TGOs were assessed by mixing *E. coli* with GO suspensions of concentrations ranging from 0 to 500 μ g/mL for 3 h. A reduction of bacterial cell viability was observed at the lower concentrations, followed by a significant decrease at higher concentrations when compared to the control (p < 0.05). Figure 1a shows that all materials inhibit 50% of the bacterial growth at different concentrations. From the dose—response data collected, the EC₅₀ values were determined to be 183 ± 33.9 , 143 ± 24.8 , 127 ± 11.0 , and $86.3 \pm 28.9 \ \mu$ g/mL for ARGO, TGO200, TGO500, and TGO800, respectively.

These results indicate that the antibacterial activities of these materials are in the order of TGO800 > TGO500 > TGO200 > ARGO, where TGO800 shows the highest toxicity and ARGO the lowest. The sigmoidal dose-response curves using both average values and individual data points are depicted in Figure S3. These results exhibit a statistical difference between the EC₅₀ values of all the thermally annealed materials compared to ARGO (Table S2). Additional statistical information and other parameters are shown in Table S3. The difference in antimicrobial properties can be attributed to the extent of oxidation of each of the materials. ARGO has the lowest extent of oxidation with a C/O ratio of 2.02 and the highest EC50 value, whereas TGO800 has the opposite trend with the highest C/O ratio of 7.19 and lowest EC₅₀ value. The relationship between these two parameters is observed in Figure 1b with an R^2 value of 0.9102. There is a linear decrease in the EC50 value as the material is reduced, indicating an increased inherent hazard.

Previous studies have shown that surface modification can play a role when determining the antimicrobial activity of GO. Akhavan and Ghaderi compared the toxicity of GO and rGO, where it was observed that rGO had a stronger antimicrobial activity against *E. coli* and *S. aureus*. Similarly, in a later study, they found that rGO prevented the proliferation of *E. coli*, whereas GO was biocompatible with the microorganism. The antimicrobial activity of GO can be subject to the changes in oxygen-containing groups, which can alter the GO surface and edges. The relationship between the EC₅₀ values and other surface functional groups was investigated and can be observed in Figure S4. Both the basal groups (% C–O) and the edge

groups (% C=O and % COOH) appear to have an effect on the antimicrobial activity. In both cases, there is a strong linear increase with R^2 values > 0.85 where the antimicrobial potency decreases as the percent of functional groups increases. These functional groups can affect bacterial interactions in two different ways. The more hydrophobic nature of annealed GO increases the microbe-GO interactions by decreasing the dispersibility of the materials, 44 while removing oxygen functionalities on the edges and basal planes can enhance electron-transfer capacity and antibacterial activity. These rGOs also introduce holes or defects in the carbon lattice because of CO and/or $\rm CO_2$ liberation and reduce surface charge and water dispersibility. 27,44 It is important to note that although the size plays a role in the GO's toxicity mechanisms, as described in previous studies, 11,16 ARGO and TGOs had a very similar lateral size and did not play a significant role when assessing the toxicity of the materials in this study.

3.3. Oxidative Stress Generated by ARGO and TGO **Materials.** The antimicrobial activity of GO can be mediated by both physical and chemical interactions that promote direct contact between the GO sheets and the bacterial cells. 4,11,45 The cell membrane is considered as the main target in these interactions. According to previous studies, oxidative stress is considered the dominant mechanism of toxicity for graphenebased nanomaterials; however, other studies in bacteria or lipid bilayer models emphasize physical mechanisms over chemical ones.^{8,44,46} Most graphene toxicity studies rely on testing multiple concentrations of GO/rGO and examining the biological response toward them (i.e., ROS generation, loss of glutathione). In this study, different fluorescent dye assays were performed at the EC₅₀ concentration for each material to better understand the mechanisms of GO interaction with bacteria. This approach integrates any potential effects of colloidal stability or hydrophobicity of the different materials by comparing them at the same biological endpoint, the EC₅₀, to better resolve the mechanisms of GO-cell interactions at the concentration where 50% of bacterial cells elucidate a response (in this case a reduction in cell viability) regardless of the material's surface chemistry.

The oxidative stress mechanism is often mediated by the generation of ROS upon bacteria—GO contact. An over-production of ROS can cause the cells to enter a state of oxidative stress that results in damage to cellular components such as proteins, lipids, and nucleic acids.⁴⁷ In this study, ROS generation was tested using a fluorescent probe (H₂DCFDA),

which is a general oxidative stress indicator and is sensitive to a wide range of free radical oxidizing species.⁴⁸ As shown in Figure 2a, ARGO, TGO500, and TGO800 increase intracellular ROS formation, as shown by 58, 14, and 13% increase in H₂DCFDA, respectively, compared to the control. Even though the annealed materials TGO500 and TGO800 had an increase in ROS, the higher ROS generation by ARGO suggests that the more oxidized the material, the higher its capacity to induce oxidative stress. Lipid peroxidation levels were measured as a biomarker to further assess oxidative stress using the BODIPY dye. However, none of the materials induced an increase of peroxidase levels when compared to the control. This discrepancy between ROS generation and lipid peroxidation suggests that although ROS formation was induced by GO exposure, the oxidative stress resulting from this exposure was either mild or targeting cellular components other than lipids.

The esterase activity responses of E. coli after ARGO and TGO exposure were quantified and are shown in Figure 2a. After a 3 h GO exposure, there is an increase in esterase activity in the two most reduced materials TGO500 and TGO800 by 30 and 42%, respectively. Increase in FDA fluorescence may be attributed to an increase in intracellular FDA concentration, which can be the result of membrane hyperpolarization ^{49,50} induced by the interactions between nanomaterials and the cell surface, 51 or an increase in dye retention because of a decrease in cell permeability in GOcovered bacterial cells. These results suggest a possible cell wrapping mechanism for the annealed GOs (TGO500 and TGO800), as observed in previous studies. 11,17,52 A comparison of all the dyes with both the positive control (5 mM CuCl₂) and the negative control (no material) is shown in Table S4.

Glutathione oxidation serves as another way to corroborate cellular oxidative stress. GSH is the most abundant lowmolecular-weight antioxidant synthesized in cells and it plays a role in keeping an intracellular oxidative equilibrium. The acellular oxidation of GSH was tested to investigate the oxidative potential of the materials. As shown in Figure 2b, the loss of GSH was measured after GSH was exposed to the GO materials at different time intervals (0-6 h). The extent of reduction of the materials influenced the GSH oxidation response. For ARGO, the most oxidized material, GSH oxidation increased from 8 to 33% after 6 h of exposure. In comparison, at 6 h exposure, the TGO materials resulted in 12, 9.6, and 9.3% GSH oxidation for TGO200, TGO500, and TGO800, respectively. The higher GSH oxidation by ARGO indicates that this material has a higher biological reactivity when compared to all TGOs even after 1 h of exposure. This change can be attributed to the higher amount of surface oxygen in ARGO. In the basal plane of GO, carbon atoms bonded with C-O-C and C-OH groups decrease from 41.89% for ARGO to 9.09% for TGO800 upon thermal annealing, which translates to a greater defect density in ARGO compared to the TGO samples. Additionally, an increase in %O enhances ARGO's dispersion in water (more active sites available) and it has an abundance of epoxy (C-O-C) groups, which are very reactive.²⁷ Previous studies have linked a higher GSH oxidation to defect density or oxidation debris in graphene materials. 11,15,27,53 ARGO, with a highly oxidized surface, facilitates the adsorption of oxygen on defect sites, generating surface oxides and eventually releasing ROS

such as peroxide (H2O2) or superoxide (O2^), promoting GSH oxidation. 11,14,27,54

The oxidative stress generated by ARGO and TGO materials has distinct responses related to their surface chemistry and oxidation extent. On one hand, the most oxidized material, ARGO, leads to the highest oxidative potential demonstrated by the highest ROS generation and GSH oxidation. Higher defect densities in ARGO may explain its higher oxidative potential. These results suggest that chemical interactions between ARGO and E. coli are more important in oxidized GO materials. On the other hand, TGOs, particularly TGO500 and TGO800, have a higher wrapping capacity than ARGO and TGO200 by decreasing the cell permeability, which suggests that a physical mechanism is the dominant mode of interaction. Although GO-bacteria interactions have been studied under various experimental conditions in previous studies, 9,29,53,55,56 this is the first study that reveals a shift in mechanism as the material's surface chemistry changes from oxidized to reduced graphene.

3.4. Mechanism of Interaction between ARGO and **TGOs toward** *E. coli.* The antimicrobial properties of GO are attributed to a combination of mechanisms as explained in the previous section. A post-exposure sonication experiment was done to examine the possibility of a wrapping mechanism between GO and bacteria. Figure 3 shows cell viability after E.

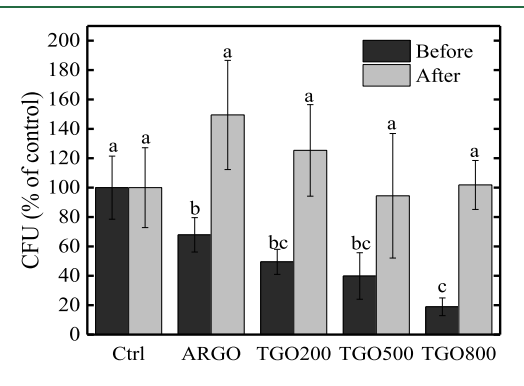


Figure 3. Viable CFU count for E. coli after 3 h of exposure to GO sheets before and after bath sonication. Plating assay results using the EC₅₀ concentration of each material before and after 10 min of bath sonication. Different letters represent statistical difference between materials at $p \le 0.05$ (n = 9). All experiments are compared to the negative control (no GO).

coli was exposed for 3 h to ARGO and TGOs in suspension at their EC50 values. As expected, all materials decrease the CFU counts significantly with respect to the control (dark gray columns). In contrast, after 10 min of bath sonication and immediate replating, results reveal no significant changes in cell viability with respect to the control.

To better understand the recovery of viable cells after sonication, epifluorescence microscopy was done to assess the cell viability of bacteria in contact with GO. Figure 4a-c shows representative epifluorescence microscopy images of E. coli stained with Syto9 and PI to show live and dead cells, respectively. As expected, the control sample had only viable cells as indicated by their bright green fluorescence (Figure 4a). After exposure to ARGO, it is observed that most of the cells are still viable, with only a few dead cells (red spot) observed. More importantly, cells are present all over the ARGO sheets and are adsorbed by the material. This is exemplified in the zoomed-in panel in Figure 4b where cells are **Environmental Science & Technology**

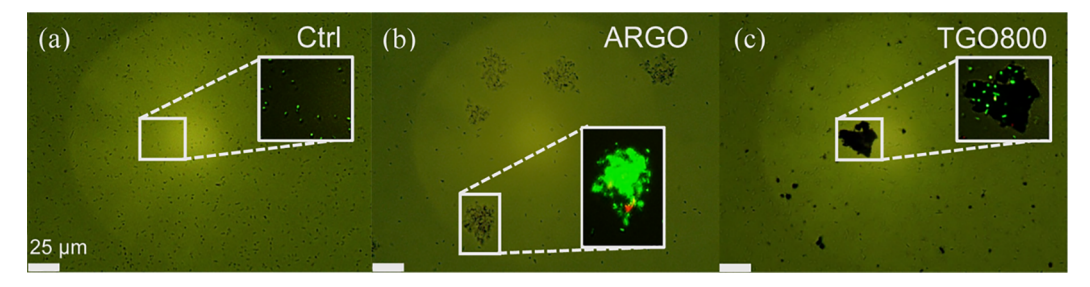


Figure 4. GO-bacteria interaction. (A-C) Representative epifluorescence microscopy images of E. coli cells after 3 h of exposure to no GO (ctrl) and 250 µg/mL of ARGO and TGO800, respectively. Main panels show bright field microscopy mode and the inset close-up panels show fluorescent mode using the green and red fluorescent channels. 1×10^8 cells/mL were stained with Syto9 and PI to show live (green) and dead (red) cells, respectively.

present where ARGO is present. Similarly, after exposure to TGO800, E. coli cells remain viable and are in close contact with the material. SEM micrographs support the adsorption abilities of GO toward E. coli as observed in Figure S5a,b. The two panels show bacteria cells in contact with welldistinguished ARGO and TGO800 sheets, respectively. These results indicate that the bacteria are trapped or adsorbed on both materials with no major physical disruption of the cell. Interestingly, ARGO and TGO800 have different morphologies; whereas ARGO is lighter and more porous and stable in aqueous solutions, TGO800 looks darker and aggregates easily, which may alter GO-bacteria interactions.

In the literature, the cell recovery is attributed to a wrapping mechanism that occurs when GO sheets act as a flexible blanket that can cover the microorganisms. This effect can isolate microorganisms from the external environment, limit access to nutrients, and prevent proliferation. 17 Cell entrapment in GO sheets was first reported by Akhavan et al. where they showed that E. coli cells could be reactivated via a mechanical separation of the sheets using sonication.¹⁷ Liu et al. 16 have shown that the sheet size impacts GO wrapping around bacteria: large GO sheets completely covered E. coli cells and prevented bacteria proliferation, whereas small GO sheets did not fully cover the cells and allowed nutrient transport. Similarly, Perreault et al. 11 observed that the number of viable cells decreased from 55 to 0.5% when the GO sheet area increased. They also observed that GO, when coated on a surface, has a different antimicrobial potency than when applied in suspension; thus, sheet orientation and way of exposure (dispersion vs static) can also impact the GObacteria interactions. 11,46,57-60 If the GO orientation is orthogonal with respect to the bacteria, the sharp edges of GO can penetrate the cells. ^{57,59} However, the epifluorescence microscopy and SEM images suggest that bacterial cells are adsorbed to the GO materials and not wrapped inside the aggregates. This conclusion is similar for both ARGO and TGO800 and reveals that cell-material interactions, rather than wrapping and isolation, are responsible for preventing bacterial growth.

3.5. Surface Chemistry Shifts the Antimicrobial Mechanisms of ARGO and TGOs. The surface chemistry of GO was found to have an important influence on its antimicrobial activity. Highly oxidized GO generated the highest response from intracellular ROS and loss of glutathione, suggesting a chemically driven GO-microbe interaction. However, the EC₅₀ value decreases as the oxygen content of the material decreases in TGOs. The lower defects in their carbon surface, despite lowering ROS formation in the

cell, promote a trapping mechanism where TGOs adsorb bacteria cells, reduce cell permeability, and prevent them from proliferating. These findings reveal an important shift in mechanism upon changes in the surface chemistry of GObased materials, with physically dominated interactions as the oxygen content decreases. This new understanding of the biological interactions of GO sheets with bacteria, which was enabled by comparing the different GO materials at the same biological effect (i.e., the EC50 value), provides useful guidelines to tailor the function of GO materials based on its chemical composition.

ASSOCIATED CONTENT

S Supporting Information

The Supporting Information is available free of charge at https://pubs.acs.org/doi/10.1021/acs.est.9b05057.

Impurities in ARGO and TGOs; XPS peak deconvolution of ARGO and TGOs; EC50 values of ARGO and TGOs; statistical data and parameters of ARGO and TGOs after sigmoidal dose-response fit; dye fluorescence of FDA, BODIPY, and ROS with statistical data; SEM micrographs and size distribution histograms of ARGO and TGO800; sigmoidal fit of dose-response curves for ARGO and TGOs; linear fit of EC50 values for ARGO and TGOs with respect to oxygen functional groups; and SEM micrographs of E. coli cells exposed to ARGO and TGO800 (PDF)

AUTHOR INFORMATION

Corresponding Author

*E-mail: francois.perreault@asu.edu.

ORCID

Yan Wang: 0000-0002-9147-1136

François Perreault: 0000-0002-4756-8205

The authors declare no competing financial interest.

ACKNOWLEDGMENTS

This work was supported by the National Science Foundation through the CBET-1708681 award and the Nanosystems Engineering Research Center for Nanotechnology-Enabled Water Treatment (EEC-1449500). A.B. acknowledges the support of a Dean's Fellowship from the Ira A. Fulton Schools of Engineering and a Scholar Award given by the International Chapter of the P.E.O. Sisterhood. The authors gratefully acknowledge the use of the characterization facilities within the Electron Microscopy division of the CLAS Bioimaging Facility

at ASU, particularly Dr. David Lowry for his help with the SEM images.

REFERENCES

- (1) Katsnelson, M. I. Graphene: Carbon in Carbon Is One of the Most Intriguing Elements in the Periodic Table. *Rev. Lat. Am. Lit. Arts* **2007**, *10*, 20–27.
- (2) Novoselov, K. S.; Geim, A. K.; Morozov, S. V.; Jiang, D.; Zhang, Y.; Dubonos, S. V.; Grigorieva, I. V.; Firsov, A. A. Electric Field Effect in Atomically Thin Carbon Films. *Science* **2004**, *306*, *666*–*669*.
- (3) Balandin, A. A. Thermal Properties of Graphene and Nanostructured Carbon Materials. *Nat. Mater.* **2011**, *10*, 569–581.
- (4) Perreault, F.; De Faria, A. F.; Elimelech, M. Environmental Applications of Graphene-Based Nanomaterials. *Chem. Soc. Rev.* **2015**, 44, 5861–5896.
- (5) De Jesus, L. R.; Dennis, R. V.; Depner, S. W.; Jaye, C.; Fischer, D. A.; Banerjee, S. Inside and Outside: X-Ray Absorption Spectroscopy Mapping of Chemical Domains in Graphene Oxide. *J. Phys. Chem. Lett.* **2013**, *4*, 3144–3151.
- (6) Rojas-Andrade, M. D.; Chata, G.; Rouholiman, D.; Liu, J.; Saltikov, C.; Chen, S. Antibacterial Mechanisms of Graphene-Based Composite Nanomaterials. *Nanoscale* **2017**, *9*, 994–1006.
- (7) Karahan, H. E.; Wang, Y.; Li, W.; Liu, F.; Wang, L.; Sui, X.; Riaz, M. A.; Chen, Y. Antimicrobial Graphene Materials: The Interplay of Complex Materials Characteristics and Competing Mechanisms. *Biomater. Sci.* **2018**, *6*, 766–773.
- (8) Al-Jumaili, A.; Alancherry, S.; Bazaka, K.; Jacob, M. V. Review on the Antimicrobial Properties of Carbon Nanostructures. *Materials* **2017**, *10*, 1066.
- (9) Carpio, I. E. M.; Santos, C. M.; Wei, X.; Rodrigues, D. F. Toxicity of a Polymer-Graphene Oxide Composite against Bacterial Planktonic Cells, Biofilms, and Mammalian Cells. *Nanoscale* **2012**, *4*, 4746–4756.
- (10) Hegab, H. M.; Elmekawy, A.; Zou, L.; Mulcahy, D.; Saint, C. P.; Ginic-Markovic, M. The Controversial Antibacterial Activity of Graphene-Based Materials. *Carbon* **2016**, *105*, 362–376.
- (11) Perreault, F.; de Faria, A. F.; Nejati, S.; Elimelech, M. Antimicrobial Properties of Graphene Oxide Nanosheets: Why Size Matters. *ACS Nano* **2015**, *9*, 7226–7236.
- (12) Zou, X.; Zhang, L.; Wang, Z.; Luo, Y. Mechanisms of the Antimicrobial Activities of Graphene Materials. *J. Am. Chem. Soc.* **2016**, 138, 2064–2077.
- (13) Di Giulio, M.; Zappacosta, R.; Di Lodovico, S.; Di Campli, E.; Siani, G.; Fontana, A.; Cellini, L. Antimicrobial and Antibiofilm Efficacy of Graphene Oxide against Chronic Wound Microorganisms. *Antimicrob. Agents Chemother.* **2018**, 62, e00547.
- (14) Gurunathan, S.; Woong Han, J.; Abdal Daye, A.; Eppakayala, V.; Kim, J.-h. Oxidative Stress-Mediated Antibacterial Activity of Graphene Oxide and Reduced Graphene Oxide in Pseudomonas Aeruginosa. *Int. J. Nanomed.* **2012**, *7*, 5901–5914.
- (15) Castrillón, S. R.-V.; Perreault, F.; De Faria, A. F.; Elimelech, M. Interaction of Graphene Oxide with Bacterial Cell Membranes: Insights from Force Spectroscopy. *Environ. Sci. Technol. Lett.* **2015**, *2*, 112–117.
- (16) Liu, S.; Hu, M.; Zeng, T. H.; Wu, R.; Jiang, R.; Wei, J.; Wang, L.; Kong, J.; Chen, Y. Lateral Dimension-Dependent Antibacterial Activity of Graphene Oxide Sheets. *Langmuir* **2012**, *28*, 12364–12372.
- (17) Akhavan, O.; Ghaderi, E.; Esfandiar, A. Wrapping Bacteria by Graphene Nanosheets for Isolation from Environment, Reactivation by Sonication, and Inactivation by near-Infrared Irradiation. *J. Phys. Chem. B* **2011**, *115*, 6279–6288.
- (18) Qu, X.; Sekol, R. C.; Taylor, A. D.; Pfefferle, L. D.; Zimmerman, J. B. Realizing Comparable Oxidative and Cytotoxic Potential of Single- and Multiwalled Carbon Nanotubes through Annealing. *Environ. Sci. Technol.* **2013**, 47, 14080–14088.
- (19) Vecitis, C. D.; Zodrow, K. R.; Kang, S.; Elimelech, M. Electronic-Structure-Dependent Bacterial Cytotoxicity of Single-Walled Carbon Nanotubes. *ACS Nano* **2010**, *4*, 5471–5479.

- (20) Jia, G.; Wang, H.; Yan, L.; Wang, X.; Pei, R.; Yan, T.; Zhao, Y.; Guo, X. Cytotoxicity of Carbon Nanomaterials: Single-Wall Nanotube, Multi-Wall Nanotube, and Fullerene. *Environ. Sci. Technol.* **2005**, 39, 1378–1383.
- (21) Pasquini, L. M.; Hashmi, S. M.; Sommer, T. J.; Elimelech, M.; Zimmerman, J. B. Impact of Surface Functionalization on Bacterial Cytotoxicity of Single-Walled Carbon Nanotubes. *Environ. Sci. Technol.* **2012**, *46*, 6297–6305.
- (22) Gilbertson, L. M.; Goodwin, D. G.; Taylor, A. D.; Pfefferle, L.; Zimmerman, J. B. Toward Tailored Functional Design of Multi-Walled Carbon Nanotubes (MWNTs): Electrochemical and Antimicrobial Activity Enhancement via Oxidation and Selective Reduction. *Environ. Sci. Technol.* **2014**, *48*, 5938–5945.
- (23) Arias, L. R.; Yang, L. Inactivation of Bacterial Pathogens by Carbon Nanotubes in Suspensions. *Langmuir* **2009**, *25*, 3003–3012.
- (24) Falinski, M. M.; Plata, D. L.; Chopra, S. S.; Theis, T. L.; Gilbertson, L. M.; Zimmerman, J. B. A Framework for Sustainable Nanomaterial Selection and Design Based on Performance, Hazard, and Economic Considerations. *Nat. Nanotechnol.* **2018**, *13*, 708–714.
- (25) Petersen, E. J.; Henry, T. B. Methodological Considerations for Testing the Ecotoxicity of Carbon Nanotubes and Fullerenes: Review. *Environ. Toxicol. Chem.* **2012**, *31*, 60–72.
- (26) Gilbertson, L. M.; Zimmerman, J. B.; Plata, D. L.; Hutchison, J. E.; Anastas, P. T. Designing Nanomaterials to Maximize Performance and Minimize Undesirable Implications Guided by the Principles of Green Chemistry. *Chem. Soc. Rev.* **2015**, *44*, 5758–5777.
- (27) Wang, Y.; Gilbertson, L. M. Informing Rational Design of Graphene Oxide through Surface Chemistry Manipulations: Properties Governing Electrochemical and Biological Activities. *Green Chem.* **2017**, *19*, 2826–2838.
- (28) Hofmann, M.; Wei, J.; Chen, Y.; Liu, S.; Zeng, T. H.; Hofmann, M.; Burcombe, E.; Wei, J.; Jiang, R. Antibacterial Activity of Graphite, Graphite Oxide, Graphene Oxide, and Reduced Graphene Oxide: Membrane and Oxidative Stress. ACS Nano 2011, 2016, 6971–6980.
- (29) Akhavan, O.; Ghaderi, E. Toxicity of Graphene and Graphene Oxide Nanowalls against Bacteria. ACS Nano 2010, 4, 5731–5736.
- (30) Zucker, I.; Werber, J. R.; Fishman, Z. S.; Hashmi, S. M.; Gabinet, U. R.; Lu, X.; Osuji, C. O.; Pfefferle, L. D.; Elimelech, M. Loss of Phospholipid Membrane Integrity Induced by Two-Dimensional Nanomaterials. *Environ. Sci. Technol. Lett.* **2017**, *4*, 404–409.
- (31) Odonkor, S. T.; Ampofo, J. K. Escherichia Coli as an Indicator of Bacteriological Quality of Water: An Overview. *Microbiol. Res.* **2013**, *4*, 2.
- (32) Chatterjee, A. K.; Chakraborty, R.; Basu, T. Mechanism of Antibacterial Activity of Copper Nanoparticles. *Nanotechnology* **2014**, 25 (). DOI: 10.1088/0957-4484/25/13/135101
- (33) Chen, Z.; Bertin, R.; Froldi, G. EC50 Estimation of Antioxidant Activity in DPPH* Assay Using Several Statistical Programs. *Food Chem.* **2013**, *138*, 414–420.
- (34) Melegari, S. P.; Perreault, F.; Costa, R. H. R.; Popovic, R.; Matias, W. G. Evaluation of Toxicity and Oxidative Stress Induced by Copper Oxide Nanoparticles in the Green Alga Chlamydomonas Reinhardtii. *Aquat. Toxicol.* **2013**, *142–143*, 431–440.
- (35) Regel, R. H.; Ferris, J. M.; Ganf, G. G.; Brookes, J. D. Algal Esterase Activity as a Biomeasure of Environmental Degradation in a Freshwater Creek. *Aquat. Toxicol.* **2002**, *59*, 209–223.
- (36) Perreault, F.; Oukarroum, A.; Melegari, S. P.; Matias, W. G.; Popovic, R. Polymer Coating of Copper Oxide Nanoparticles Increases Nanoparticles Uptake and Toxicity in the Green Alga Chlamydomonas Reinhardtii. *Chemosphere* **2012**, 87, 1388–1394.
- (37) Ellman, G. L. Tissue Sulfhydryl Groups. Arch. Biochem. Biophys. 1959, 82, 70-77.
- (38) Ganguly, A.; Sharma, S.; Papakonstantinou, P.; Hamilton, J. Probing the Thermal Deoxygenation of Graphene Oxide Using High-Resolution in Situ X-Ray-Based Spectroscopies. *J. Phys. Chem. C* **2011**, *115*, 17009–17019.
- (39) Amadei, C. A.; Arribas, P.; Vecitis, C. D. Graphene Oxide Standardization and Classification: Methods to Support the Leap from Lab to Industry. *Carbon* **2018**, *133*, 398–409.

- (40) Yang, D.; Velamakanni, A.; Bozoklu, G.; Park, S.; Stoller, M.; Piner, R. D.; Stankovich, S.; Jung, I.; Field, D. A.; Ventrice, C. A.; Ruoff, R. S. Chemical Analysis of Graphene Oxide Films after Heat and Chemical Treatments by X-Ray Photoelectron and Micro-Raman Spectroscopy. *Carbon* **2009**, *47*, 145–152.
- (41) Mattevi, C.; Eda, G.; Agnoli, S.; Miller, S.; Mkhoyan, K. A.; Celik, O.; Mastrogiovanni, D.; Granozzi, G.; Garfunkel, E.; Chhowalla, M. Evolution of Electrical, Chemical, and Structural Properties of Transparent and Conducting Chemically Derived Graphene Thin Films. *Adv. Funct. Mater.* **2009**, *19*, 2577–2583.
- (42) Lerf, A.; He, H.; Forster, M.; Klinowski, J. Structure of Graphite Oxide Revisited . **1998**, *102*, 4477–4482. DOI: 10.1021/jp9731821
- (43) Akhavan, O.; Ghaderi, E. Escherichia Coli Bacteria Reduce Graphene Oxide to Bactericidal Graphene in a Self-Limiting Manner. *Carbon* **2012**, *50*, 1853–1860.
- (44) Sanchez, V. C.; Jachak, A.; Hurt, R. H.; Kane, A. B. Biological Interactions of Graphene-Family Nanomaterials: An Interdisciplinary Review. *Chem. Res. Toxicol.* **2012**, 25, 15–34.
- (45) Nanda, S. S.; Yi, D. K.; Kim, K. Study of Antibacterial Mechanism of Graphene Oxide Using Raman Spectroscopy. *Sci. Rep.* **2016**, *6*, 1–12.
- (46) Lu, X.; Feng, X.; Werber, J. R.; Chu, C.; Zucker, I.; Kim, J.-H.; Osuji, C. O.; Elimelech, M. Enhanced Antibacterial Activity through the Controlled Alignment of Graphene Oxide Nanosheets. *Proc. Natl. Acad. Sci. U.S.A.* **2017**, *114*, E9793–E9801.
- (47) Krishnamoorthy, K.; Veerapandian, M.; Zhang, L.-H.; Yun, K.; Kim, S. J. Antibacterial Efficiency of Graphene Nanosheets against Pathogenic Bacteria via Lipid Peroxidation. *J. Phys. Chem. C* **2012**, *116*, 17280–17287.
- (48) Hempel, S. L.; Buettner, G. R.; O'Malley, Y. Q.; Wessels, D. A.; Flaherty, D. M. Dihydrofluorescein Diacetate Is Superior for Detecting Intracellular Oxidants: Comparison with 2',7'-Dichlorodihydrofluorescein Diacetate, 5(and 6)-Carboxy-2',7'-Dichlorodihydrofluorescein Diacetate, and Dihydrorhodamine 123. Free Radic. Biol. Med. 1999, 27, 146–159.
- (49) Franklin, N. M.; Adams, M. S.; Stauber, J. L.; Lim, R. P. Development of an Improved Rapid Enzyme Inhibition Bioassay with Marine and Freshwater Microalgae Using Flow Cytometry. *Arch. Environ. Contam. Toxicol.* **2001**, *40*, 469–480.
- (50) Franklin, N. M.; Stauber, J. L.; Lim, R. P. Development of Flow Cytometry-Based Algal Bioassays for Assessing Toxicity of Copper in Natural Waters. *Environ. Toxicol. Chem.* **2001**, 20, 160–170.
- (51) Miyazawa, N.; Hakamada, M.; Mabuchi, M. Antimicrobial Mechanisms Due to Hyperpolarisation Induced by Nanoporous Au. *Sci. Rep.* **2018**, *8*, 1–8.
- (52) Chen, J.; Peng, H.; Wang, X.; Shao, F.; Yuan, Z.; Han, H. Graphene Oxide Exhibits Broad-Spectrum Antimicrobial Activity against Bacterial Phytopathogens and Fungal Conidia by Intertwining and Membrane Perturbation. *Nanoscale* **2014**, *6*, 1879–1889.
- (53) Faria, A. F.; Perreault, F.; Elimelech, M. Elucidating the Role of Oxidative Debris in the Antimicrobial Properties of Graphene Oxide. *ACS Appl. Nano Mater.* **2018**, *1*, 1164–1174.
- (54) Liu, X.; Sen, S.; Liu, J.; Kulaots, I.; Geohegan, D.; Kane, A.; Puretzky, A. A.; Rouleau, C. M.; More, K. L.; Palmore, G. T. R.; Hurt, R. H. Antioxidant Deactivation on Graphenic Nanocarbon Surfaces. *Small* **2011**, *7*, 2775–2785.
- (55) Santos, C. M.; Tria, M. C. R.; Vergara, R. A. M. V.; Ahmed, F.; Advincula, R. C.; Rodrigues, D. F. Antimicrobial Graphene Polymer (PVK-GO) Nanocomposite Films. *Chem. Commun.* **2011**, 47, 8892–8894.
- (56) Mangadlao, J. D.; Santos, C. M.; Felipe, M. J. L.; De Leon, A. C. C.; Rodrigues, D. F.; Advincula, R. C. On the Antibacterial Mechanism of Graphene Oxide (GO) Langmuir-Blodgett Films. *Chem. Commun.* **2015**, *51*, 2886–2889.
- (57) Palmieri, V.; Lauriola, M. C.; Ciasca, G.; Conti, C.; De Spirito, M.; Papi, M. The Graphene Oxide Contradictory Effects against Human Pathogens. *Nanotechnology* **2017**, *28*, 152001.
- (58) Li, Y.; Yuan, H.; von dem Bussche, A.; Creighton, M.; Hurt, R. H.; Kane, A. B.; Gao, H. Graphene Microsheets Enter Cells through

- Spontaneous Membrane Penetration at Edge Asperities and Corner Sites. *Proc. Natl. Acad. Sci. U.S.A.* **2013**, *110*, 12295–12300.
- (59) Hui, L.; Piao, J.-G.; Auletta, J.; Hu, K.; Zhu, Y.; Meyer, T.; Liu, H.; Yang, L. Availability of the Basal Planes of Graphene Oxide Determines Whether It Is Antibacterial. *ACS Appl. Mater. Interfaces* **2014**, *6*, 13183–13190.
- (60) Xue, J.; BinAhmed, S.; Wang, Z.; Karp, N. G.; Stottrup, B. L.; Romero-Vargas Castrillón, S. Bacterial Adhesion to Graphene Oxide (GO)-Functionalized Interfaces Is Determined by Hydrophobicity and GO Sheet Spatial Orientation. *Environ. Sci. Technol. Lett.* **2018**, *5*, 14–19.